Available online at www.sciencedirect.com
SCIENCE DIRECT
Journal of Solid State Chemistry 179 (2006) 1792–1801
JOURNAL OF SOLID STATE CHEMISTRY
www.elsevier.com/locate/jssc

Nanostructural drug-inorganic clay composites: Structure, thermal property and in vitro release of captopril-intercalated Mg–Al-layered double hydroxides

Hui Zhang, Kang Zou, Shaohuan Guo, Xue Duan*

State Key Laboratory of Chemical Resource Engineering, Beijing University of Chemical Technology, Box 98, Beijing 100029, China

Received 27 December 2005; received in revised form 7 March 2006; accepted 10 March 2006
Available online 24 March 2006

Abstract

A nanostructural drug-inorganic clay composite involving a pharmaceutically active compound captopril (Cpl) intercalated Mg–Al-layered double hydroxides (Cpl-LDHs) with Mg/Al molar ratio of 2.06 has been assembled by coprecipitation method. Powder X-ray diffraction (XRD), Fourier transform infrared spectra (FT-IR) and Raman spectra analysis indicate a successful intercalation of Cpl between the layers with a vertical orientation of Cpl disulphide-containing S–S linkage. SEM photo indicates that as-synthesized Cpl-LDHs possess compact and non-porous structure with approximately and linked elliptical shape particles of ca. 50 nm. TG-DTA analyses suggest that the thermal stability of intercalated organic species is largely enhanced due to host–guest interaction involving the hydrogen bond compared to pure form before intercalation. The in vitro release studies show that both the release rate and release percentages markedly decrease with increasing pH from 4.60 to 7.45 due to possible change of release mechanism during the release process. The kinetic simulation for the release data, and XRD and FT-IR analyses for samples recovered from release media indicate that the dissolution mechanism is mainly responsible for the release behaviour of Cpl-LDHs at pH 4.60, while the ion-exchange one is responsible for that at pH 7.45.

Keywords: Layered double hydroxides; Captopril; Drug-inorganic composite; Thermal stability; Intercalation; In vitro release

1. Introduction

Organic–inorganic nanocomposites have been recognized as one of the most promising research fields in material chemistry [1]. Recently, organo-layered double hydroxides, as an important subject in the area of organic–inorganic nanocomposites, have deeply fascinated chemists due to their unique properties [2–5].

Layered double hydroxides (LDHs), also known as anionic clays, are a class of host–guest layered solids with the general formula $[M^{2+}_{1-x}M^{3+}_{x}(OH)_2]^{x+}A^{n-}_{x/n}\cdot mH_2O$, where M^{2+} and M^{3+} are di- and trivalent metal cations, A^{n-} denotes organic or inorganic anion with negative charge n, m is the number of interlayer water and x $(=M^{3+}/(M^{2+}+M^{3+}))$ is the layer charge density of LDHs [5,6]. A wide variety of LDHs can be obtained by the variation of cations M^{2+} and M^{3+} and the intercalated anion A^{n-}, and some LDHs are biocompatible [5,7,8]. Owing to the intercalation property of LDHs, many LDH compounds with intercalated beneficial organic anions, such as DNA [8–11], amino acid [12–16], pesticide [17,18], plant growth regulators [19] and drugs, [3,5,20–23] have been prepared. Particularly, much attention has been focused on the organic–inorganic LDH hybrid-containing drug molecules because of its unique properties, such as enhanced dissolution property [3,24], increased thermal stability [25,26] and controlled release rate [3,20,21]. Once encapsulated, the drugs can be released at a rate depending on the pH of the release media [3,19].

Hussein et al. [19] reported the α-naphthalene-acetate (NAA)-intercalated Zn–Al-LDH and its release property, and found that the highest release rate and release percentage were achieved from a highly acidic or highly

*Corresponding author. Fax: +86 10 6442 5385.
E-mail address: duanx@mail.buct.edu.cn (X. Duan).

0022-4596/$ - see front matter © 2006 Elsevier Inc. All rights reserved.
doi:10.1016/j.jssc.2006.03.019

alkaline media and that the release of NAA from the lamella of intercalate was controlled by the first-order kinetic during the time at the least from the beginning of the release test up to 8 h. Ambrogi et al. [20] studied diclofenac-intercalated Mg–Al-LDHs and its release process. The amount of diclofenac released in phosphate buffer at pH 7.0 was less than 70% after 10 h. The kinetic analysis shows the importance of the diffusion through the particle in controlling the drug release rate. Tronto et al. [27] investigated citrate-intercalated Mg–Al-LDHs and found that the citrate release is due to the destruction of the layers by acid attack. Wei et al. [25] reported the Mg–Al-LDHs with intercalated naproxen by ion-exchange method and mainly discussed its thermal property, indicating its potential application as the basis of a novel drug reservoir. Recently, we investigated magnetic organo-LDH systems involving the 5-aminosalicylicacid (5-ASA)-intercalated Zn–Al-LDHs coated on magnetic ferrite and found a further enhanced thermal stability of 5-ASA after simultaneous intercalation between the LDH layers and coating on $MgFe_2O_4$ cores [26].

In the present study, captopril (Cpl), 1-[(2S)-3-mercaptp-2-methyl-1-oxypropyl]-L-proline ($C_9H_{15}NO_3S$), an angiotensin-converting enzyme inhibitor widely used to treat hypertensive disease [28,29], was selected as a model drug and intercalated into Mg–Al-LDHs successfully by coprecipitation technique. We focus on the structure, thermal property and slow/controlled release property of as-synthesized drug–LDH composite intended for providing basic data for organic–inorganic LDH hybrids. In addition, the possible release kinetic mechanism involved is also studied.

2. Experimental

2.1. Materials

Captopril ($C_9H_{15}NO_3S$, molecular weight 217, abbreviated as Cpl here) was purchased from Changzhou Pharmaceutical Co. Ltd. (China), and used as received. Other reagents were all of analytical grade (AR) and purchased from Beijing Yili Fine Chemical Co. and used without further purification. Deionized water was decarbonated by boiling and bubbling N_2 before employing in all synthesis steps.

2.2. Synthesis

2.2.1. Synthesis of Cpl-intercalated Mg–Al-LDHs

An aqueous solution (100 mL) containing NaOH (1.52 g, 0.038 mol) and Cpl (2.61 g, 0.012 mol) was added dropwise to a solution (250 mL) containing $Mg(NO_3)_2 \cdot 6H_2O$ (3.08 g, 0.012 mol) and $Al(NO_3)_3 \cdot 9H_2O$ (2.25 g, 0.006 mol) (initial Mg/Al = 2.0) under nitrogen atmosphere with vigorous stirring until the final pH of ca. 10. The resulting slurry was aged at 25 °C for 48 h. Then the resultant was filtered, washed with water until the pH of ca. 7 and finally dried in vacuo at room temperature for 48 h. The product was denoted as Cpl-LDHs.

2.2.2. Synthesis of NO_3-containing Mg–Al-LDHs

An aqueous solution (100 mL) containing NaOH (11.20 g, 0.28 mol) was added dropwise to a solution (160 mL) containing $Mg(NO_3)_2 \cdot 6H_2O$ (30.77 g, 0.12 mol), $Al(NO_3)_3 \cdot 9H_2O$ (22.60 g, 0.06 mol) and $NaNO_3$ (9.06 g, 4.45 mol) (initial Mg/Al = 2.0) under nitrogen atmosphere with vigorous stirring until the final pH of ca. 10. The resulting slurry was aged at 70 °C for 24 h, was then filtered and washed with water until the pH of ca. 7 and was finally dried at 60 °C for 8 h giving the product NO_3-LDHs.

2.3. Characterizations

Powder X-ray diffraction (XRD) was obtained on a Shimadzu XRD-6000 powder X-ray diffractometer under the following conditions: 40 kV, 30 mA, Cu$K\alpha$ radiation ($\lambda = 1.542$ Å) and scanning rate of 5°/min in the range of 3–70°. Fourier transform infrared spectra (FT-IR) were obtained on a Bruker Vector 22 spectrophotometer in the range of 4000–400 cm^{-1} with 2 cm^{-1} resolution by using the standard KBr disk method (sample/KBr = 1/100). The Raman spectrum was obtained on a JY-T64000 spectrometer (French) with 1 cm^{-1} resolution and the excitation source of a solid laser (500 mW, $\lambda = 532$ nm, Coherent Co., USA). A homemade PCT-1A thermal analysis system with a heating rate of 10 °C/min in air atmosphere was used to determine the thermal property of Cpl-LDHs. Metal and sulphur elemental analysis was conducted by inductively coupled plasma (ICP) emission spectroscopy on a Shimadzu ICPS-7500 instrument. CHN elemental microanalyses were obtained on an Elementar Vario elemental analyser. The SEM micrograph was recorded on a Hitachi S-3500N scanning electron microscope.

2.4. In vitro drug release

A solution-simulated gastrointestinal and intestinal fluid at pH 4.60 and 7.45 without pancreatine (phosphate-buffered solution) was employed as release medium, respectively. The release of Cpl from Cpl-LDHs into the media was performed by adding about 0.2 g Cpl-LDHs into 100 mL release medium at 37 ± 1 °C. The paddle rotation speed was 100 rpm. A sample of 2 mL was withdrawn at predetermined intervals and centrifuged. The accumulated amount of Cpl released into the solution was measured momentarily using UV–Vis spectrophotometer at 205 nm.

3. Results and discussion

3.1. Dissociation property of Cpl

Dissociation of Cpl in water involves two steps arising from the presence of an –SH function and a carboxyl

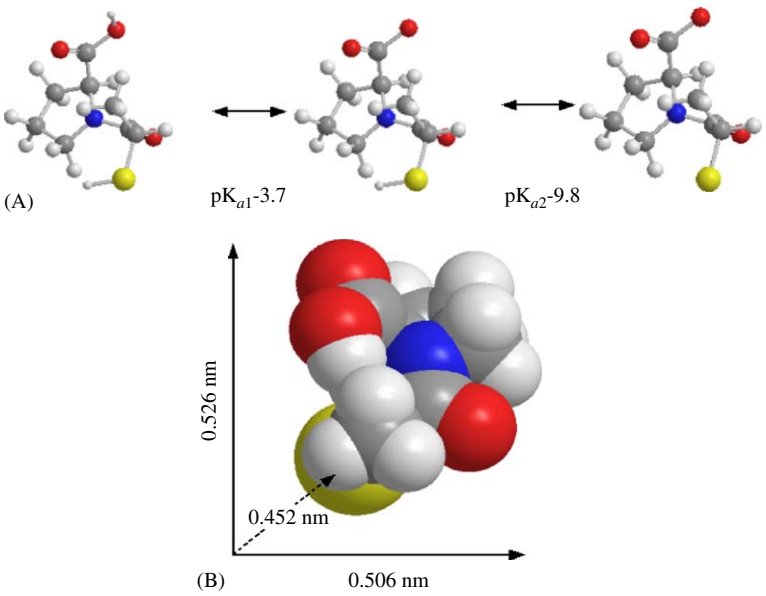

Fig. 1. (a) Dissociation of Cpl in water and (b) three-dimensional molecular size of Cpl.

function in its structure as illustrated in Fig. 1(a). The values of pK_a are $K_{a1} = 3.7$ (–COOH) and p$K_{a2} = 9.8$ (–SH) [30,31]. According to the pH of the solution and pK_a values of Cpl, the distribution coefficient δ can be calculated. On the basis of the synthesis condition with pH 10, the calculated values of δ are $\delta_0 = 3.16 \times 10^{-5}\%$ ($C_9H_{15}NO_3S$), $\delta_1 = 38.16\%$ $[C_9H_{14}NO_3S]^-$ and $\delta_2 = 61.38\%$ $[C_9H_{13}NO_3S]^{2-}$. Fig. 1(b) shows the three-dimensional molecular size of Cpl estimated by the software Chemoffice2004.

3.2. Crystal structure and chemical composition of LDH compounds

The XRD patterns of Cpl-LDHs and NO_3-LDHs are shown in Fig. 2. The three intense lines in XRD patterns at low 2θ angle correspond to diffraction by planes (003), (006) and (009) and the peak between 60 and 65° (2θ) is due to (110) plane [6]. These sharp and symmetric peaks demonstrate the formation of a single well-crystallized Mg–Al-LDHs. The interlayer distance d_{003} value, representing the combined thickness of the brucite-like layer (0.48 nm) and the gallery height, is a function of the number, the size and the orientation of intercalated anions [6]. For Cpl-LDHs (Fig. 2a), the characteristic reflections of LDH compounds, and the basal reflection (003) shift to lower 2θ angles (for (003) reflection: $2\theta = 6.04°$) as compared with that of NO_3-LDHs (Fig. 2b, $2\theta = 9.69°$), indicating the intercalation of Cpl between the LDH layers [2–5]. It can also be carefully seen that d_{003} of 1.462 nm and d_{006} of 0.740 nm of Cpl-LDHs accord to the good multiple relationship between the basal and second-order reflections as $d_{003} = 2d_{006}$ of LDH compound.

The FT-IR spectra of Cpl and Cpl-LDHs with reference to NO_3-LDHs are shown in Fig. 3. The FT-IR spectrum of Cpl as reference in Fig. 3a can be attributed as follows [31]: (1) 2980–2880 cm^{-1} to C–H stretching vibration; (2) 2566 cm^{-1} to S–H stretching vibration; (3) 1748 cm^{-1} to the COOH group and (4) 878 cm^{-1} to CH_2 rocking. For Cpl-LDHs (Fig. 3b), indicatives of Cpl intercalated in LDHs interlayer space are clearly observed. The broad absorption bands at ca. 3400 cm^{-1} arise from the stretching mode of OH groups in the brucite-like layer and physisorbed water. The bands in the range of 2980–2880 cm^{-1} are attributed to C–H stretching vibration of intercalated Cpl anions, quite similar to that of Cpl (Fig. 3a). However, the band at 1748 cm^{-1} due to the COOH group disappears, while the two bands at ca. 1589 and 1402 cm^{-1} due to the anti-symmetric and symmetric stretching vibrations of $-CO_2^-$ appear and shift to lower wavenumber, compared to free $-CO_2^-$ in Cpl [31], indicating that the intercalation of Cpl in the interlayer space involves hydrogen bonding, besides the obvious electrostatic attraction between the electropositive cations in layer and organic anions in interlayer. And generally, the band at ca. 552 cm^{-1} is attributed to *M*–O and *M*–O–H stretching vibrations of Cpl-LDHs, which locates at ca. 20 cm^{-1} smaller than that of NO_3-LDHs (Fig. 3c, 572 cm^{-1}), also confirming the existence of host–guest interaction between the interlayer Cpl anions and hydroxyl groups of LDH layers. While, the deformation band of interlayer water is likely to be overlapped by the broad band of anti-symmetric stretching vibrations of $-CO_2^-$. In addition, the band in 2600–2500 cm^{-1} due to ν(S–H) disappears (Fig. 3b), which is associated with the dissociation of S–H group of Cpl at the synthesis pH.

The Raman spectrum of Cpl-LDHs shown in Fig. 4 gives further evidence. Cpl in alkaline aqueous solution may undergo oxidative degradation at its thiol function to yield Cpl disulphide [31]. In fact, the ν(S–H) band at ~2570 cm^{-1}

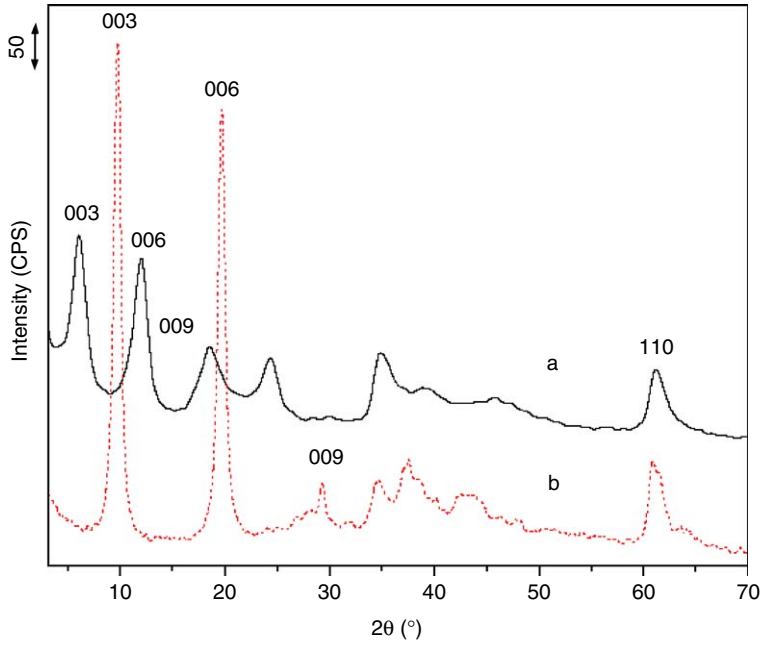

Fig. 2. The XRD patterns for Cpl-LDHs (a) and NO_3-LDHs (b).

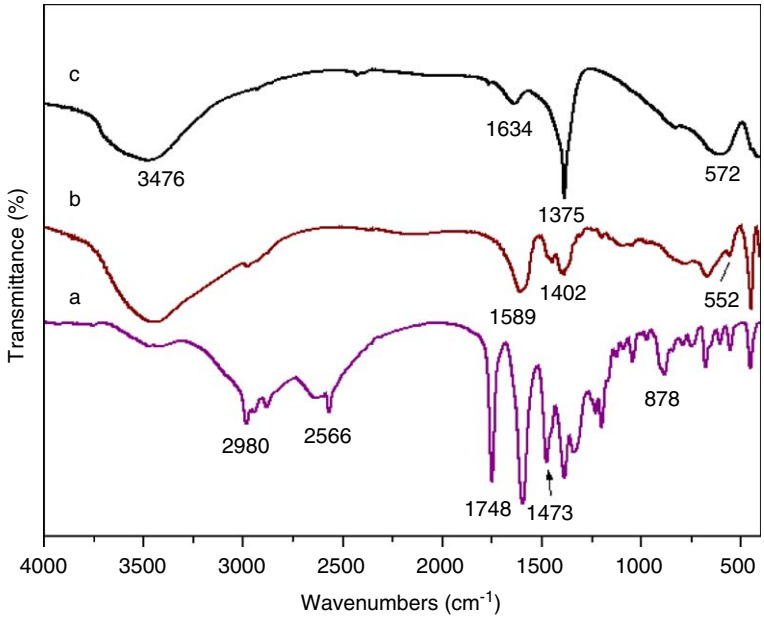

Fig. 3. The FT-IR spectra for Cpl (a), Cpl-LDHs (b) and NO_3-LDHs (c).

disappears in Fig. 4, whereas two new bands are visible in the 715–500 cm^{-1} range; the vibrations at 510 and 711 cm^{-1} can be assigned to ν(S–S) and ν(C–S), respectively [32], suggesting that the Cpl is more likely to form disulphide metabolites with S–S bond in interlayer. As for this point, Kok et al. [33] suggest that Cpl undergoes rapid oxidation to disulphide both in vitro and in vivo, like other thiols, and the disulphide metabolites can be reduced intracellularly to the free thiol and as such these can act as a reservoir for free Cpl. Therefore, it can be envisaged that Cpl intercalated in Mg–Al-LDH interlayer domain as disulphide form can also be a tunable promising reservoir for free thiol form Cpl.

Given the thickness of 0.48 nm for Mg–Al-layer [6], the interlayer spacing of Cpl-LDHs is estimated as 0.982 nm, which is 0.456 nm larger than the molecular size of Cpl (0.526 nm in Fig. 1(b)), but close to that of Cpl disulphide metabolites, implying a vertical orientation of Cpl disulphide between the layers, that is, with the carboxylate anions to both hydroxide layers with hydrogen bond. A schematic supramolecular structure of Cpl-LDHs is tentatively proposed and presented in Fig. 5.

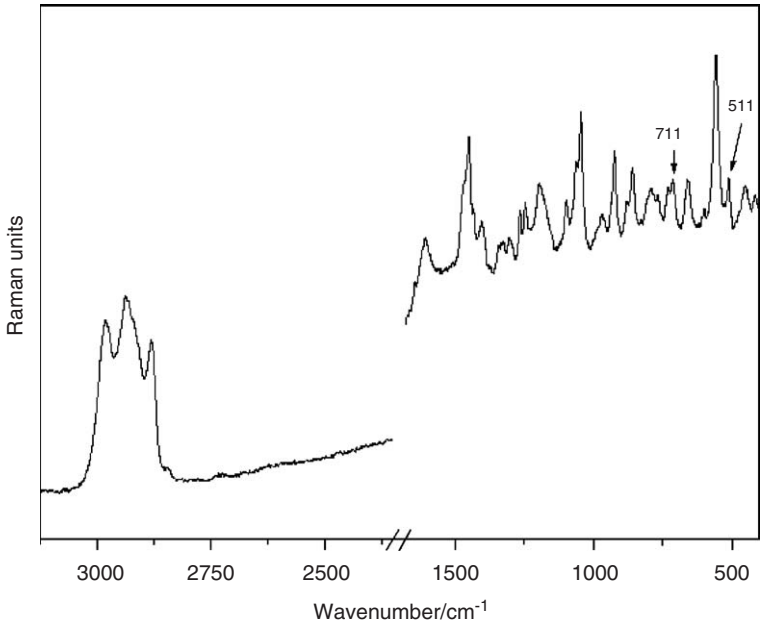

Fig. 4. Raman spectrum of Cpl-LDHs.

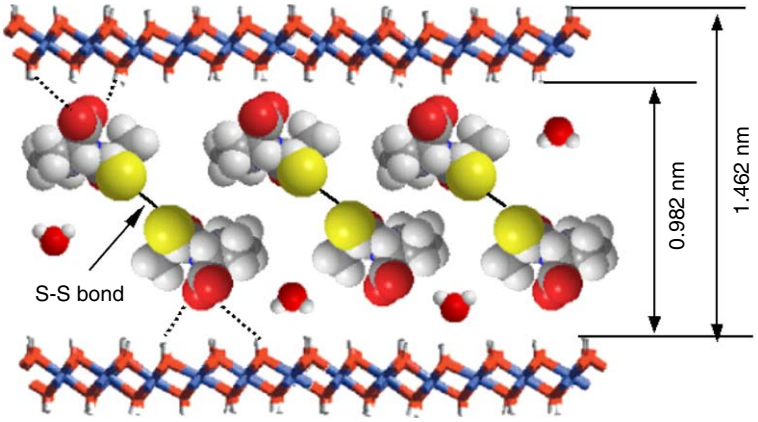

Fig. 5. Supramolecular structural model of Cpl-LDHs.

The morphology of Cpl-LDHs revealed by SEM is shown in Fig. 6. It presents compact and non-porous structure with approximately and linked ellipse-like shape particles of ca. 50 nm. Some agglomerates are also observed due to the modification of LDHs surface by organic compound intercalation [2,19].

On the basis of ICP, CHN and UV–Vis analyses, a formula of Cpl-LDHs is derived as $[Mg_{0.67}Al_{0.33}(OH)_2]^{0.33+}$ $([C_9H_{13}NO_3S\text{–}SNO_3C_9H_{13}]^{2-})_{0.065}$ $(CO_3^{2-})_{0.027}\cdot 0.53H_2O$, where small amount of CO_3^{2-} between the layers is probably due to difficulty in completely avoiding contamination from air. As shown in Table 1, the calculated values are in good agreement with the experimental data. Moreover, the UV–Vis measurement gives quite similar Cpl loading in Cpl-LDHs to that from ICP measurement.

3.3. Thermal stability

As one of the most important physical–chemical properties of organic–inorganic LDH compound, the thermal stability of Cpl-LDHs is studied initially. The TG-DTA profiles of Cpl and Cpl-LDHs are depicted in Fig. 7. In the case of pure Cpl (Fig. 7a), three main thermal events are clearly observed. The decomposition of Cpl proceeds with turbulence formation, involving processes of product vaporization [34]. The first slow event in the temperature region 90–120 °C is attributed to the Cpl melting, which corresponds to a sharp endothermic peak at ca. 108 °C; and the followed stage (200–400 °C) is due to the decomposition and subtle combustion of Cpl, which corresponds to a weak endothermic peak at ca. 267 °C and a small radiative one at ca. 302 °C. The last stage (400–600 °C) is due to the

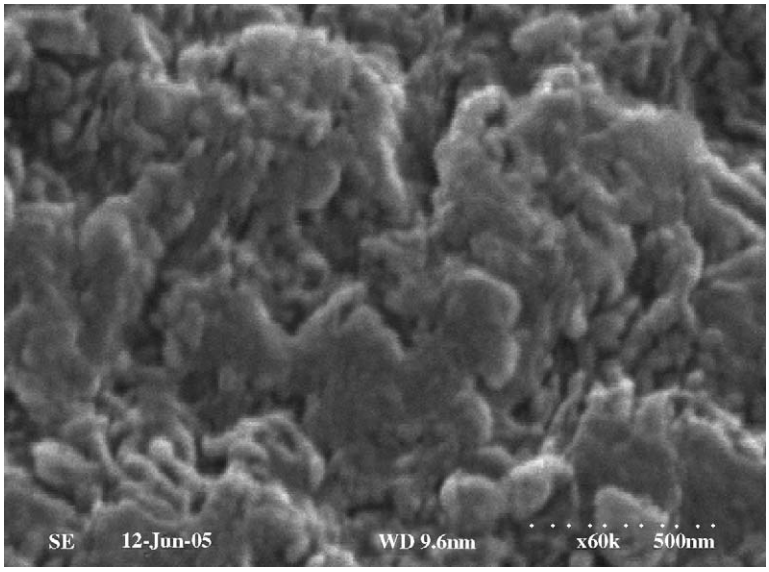

Fig. 6. The SEM image of Cpl-LDHs.

Table 1
Chemical compositions of Cpl-LDHs

	Mg%	Al%	S%	C%	H%	N%	Cpl loading %
Determined	16.25[a]	8.89[a]	4.50[a]	12.90[b]	4.77[b]	1.72[b]	31.11[a] (30.23[c])
Calculated	16.25	8.91	4.34	14.98	4.84	1.88	29.44

[a]Based on ICP analysis.
[b]Based on CHN elemental analysis.
[c]Based on UV–Vis measurement.

strong combustion of Cpl, corresponding to a sharp exothermic peak at ca. 487 °C.

However, the TG-DTA curves of Cpl-LDHs (Fig. 7b) reveal five distinguishable weight loss steps. The first and second steps between 50 and 180 °C are attributed to the removal of surface physisorbed water molecules and intercalated structure water, respectively. Correspondingly, the DTA curve shows two endothermic peaks at ca. 91 and 150 °C. The followed mass loss (180–300 °C) corresponds to a broad DTA effect between 180 and 250 °C and is due to the removal of residual intercalated water and trace dehydroxylation of the LDH layer. The mass loss in 300–500 °C corresponds to a broad radiative peak at ca. 318 °C, and is mainly attributed to the dehydroxylation of the LDH layer accompanying with the formation of layered double oxide [27,35] and the partial decomposition/combustion of intercalated Cpl disulphide under air atmosphere. It should be noticed that this temperature region is obviously higher than that of the pure free Cpl, suggesting that the thermal stability of organic Cpl species in Cpl-LDHs are clearly enhanced due to the host–guest interaction involving the hydrogen bond demonstrated previously by IR analysis. The last weak but distinguishable mass loss (500–600 °C) corresponds to a sharp exothermic peak at ca. 556 °C, and can be attributed to the major decomposition/combustion of intercalated Cpl disulphide. Moreover, from TG curve, the mass loss in 300–600 °C of Cpl-LDHs (38.3%), which is much more than UV-measured Cpl loading and elemental analysis (30.23% and 29.44% in Table 1), is inferred. This is because the dehydroxylation of LDH layer was incorporated in this temperature region. Compared to the melting/vaporization and decomposition temperature of pure Cpl, the thermal stability of Cpl is greatly improved after intercalation between the LDH layers, implying that Mg–Al-LDHs can be used as an alternative inorganic matrix for storing organic drug molecules.

3.4. In vitro drug release of Cpl-LDHs

The in vitro release properties of the drug have been investigated by adding the intercalation compound to samples of simulated gastrointestinal and intestinal fluid. Fig. 8 shows the release profiles of Cpl-LDHs in solutions at pH 7.45 and 4.60, respectively. The release behaviour at pH 4.60 is very fast during the first 1 min, which can be attributed to the partial dissolution of LDH layer at weak acidic solutions [3,19]. Thereafter a slower release step characterized as released percentage of ca. 66.7%, 85.1% and 94.2% after 1, 10 and 140 min, respectively, occurred

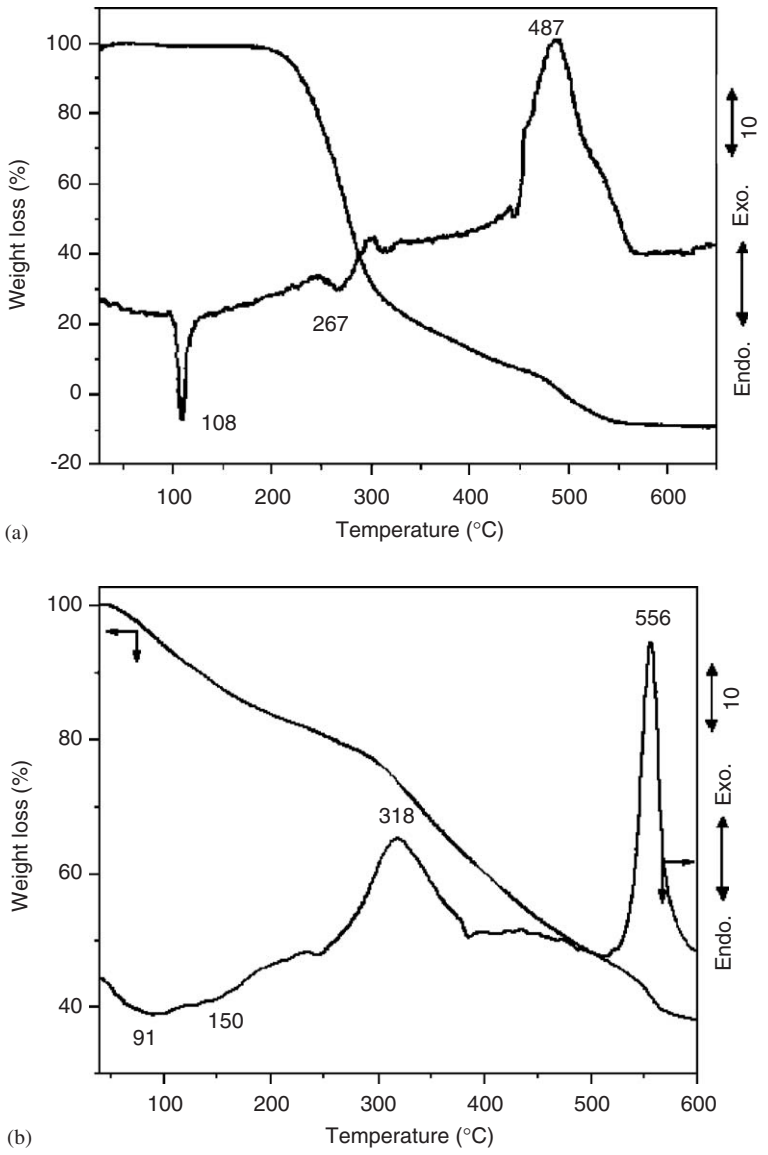

Fig. 7. The TG-DTA curves for Cpl (a) and Cpl-LDHs (b).

however. This followed slow release step may be due to an ion-exchange process between the intercalated anions in interlayer and phosphate anions in the buffer [19,20,26]. At pH 7.45, the release of Cpl-LDHs is a slow and persistent process, and ca. 12.8%, 47.4% and 92.4% of released percentage is obtained after 1, 10 and 140 min, respectively. It is worth noticing that there is no burst phenomenon happened at the beginning of release test. This slow and sustained release process may also be interpreted on the basis of the ion-exchange process between the intercalated anions and phosphate anions in the buffer [19,20,26]. On the basis of the release profiles at pH 4.60 and 7.45, it is found that the equilibrium percentage of Cpl released is not up to 100%. This is probably due to the characteristic of ion-exchange reaction [5,36,37], i.e. this is an equilibrium process and the interlayer anions cannot be exchanged completely, but the released organic species was removed or consumed continuously.

The drug release based on drug–LDHs system could be controlled either by dissolution of LDH particles [19,20], or by diffusion through the LDH particle [20]. According to literature [38,20], when the drug release fraction is slower than 0.85, Bhaskar equation shown in Eq. (1) can be used to evaluate whether the diffusion through the particle is the rate-limiting step. Thus, the release profiles were fitted by Bhaskar equation, together with the first-order equation (in Eq. (2)), which is normally used to describe the dissolution phenomena

$$-\log(1-X)\sim t^{0.65}, \tag{1}$$

$$-\log(1-X)\sim t, \tag{2}$$

where X and t are the release percentage and release time, respectively.

The fitting results are shown in Fig. 9. At pH 4.60, the release of Cpl-LDHs did not follow both equations

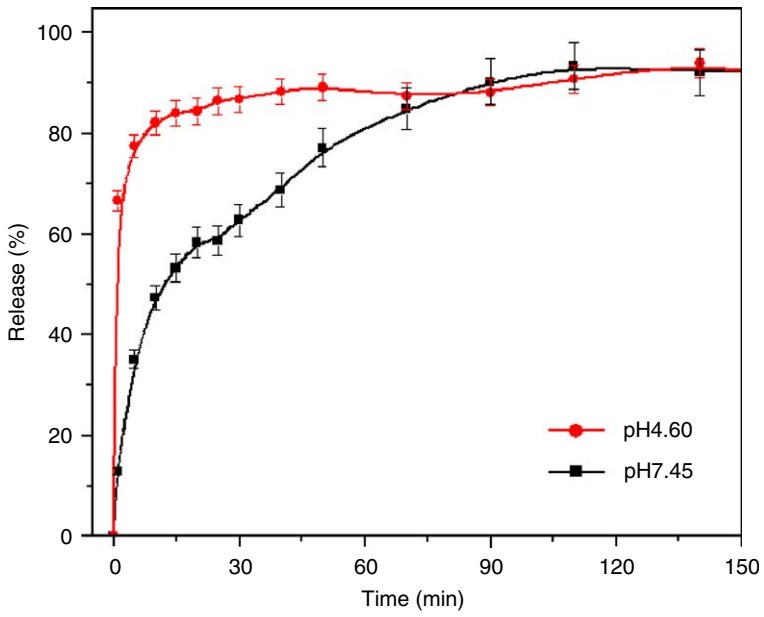

Fig. 8. Release profiles of Cpl from Cpl-LDHs in buffer solutions at different pH values.

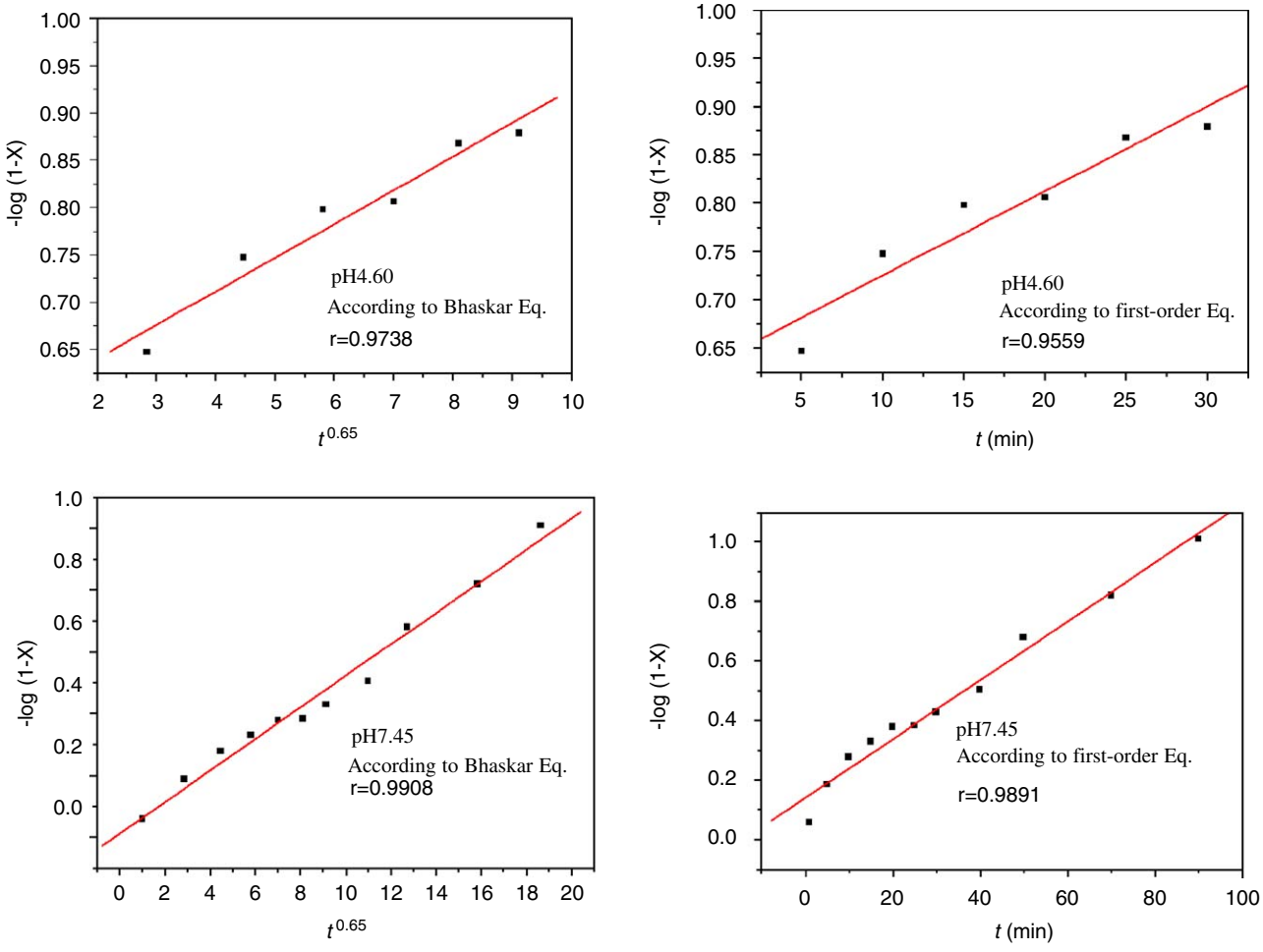

Fig. 9. Fitting the Cpl release data to different kinetic equations.

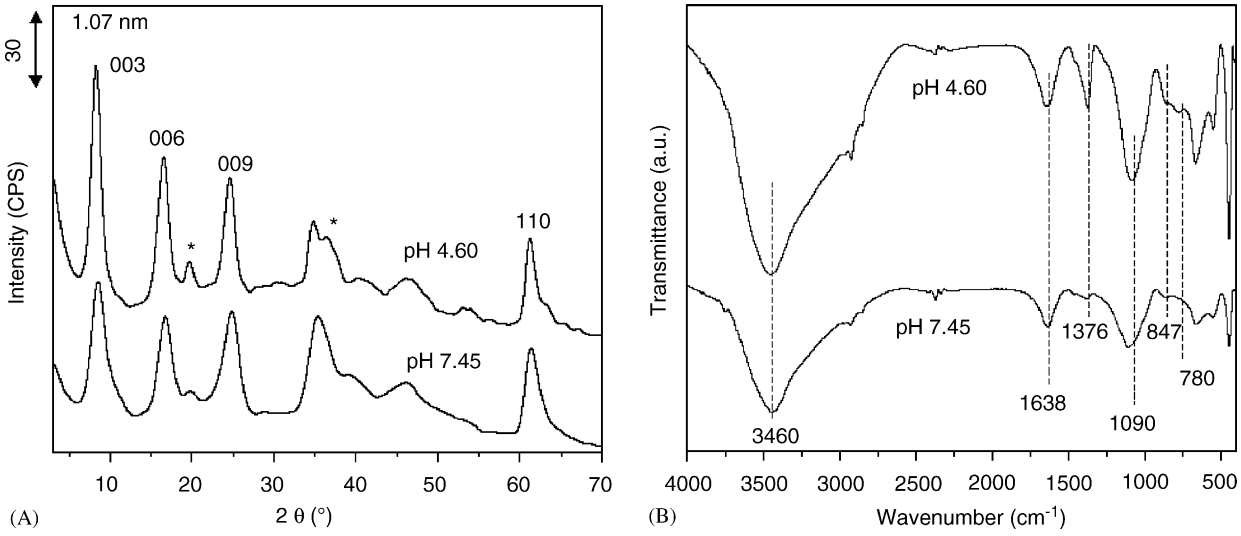

Fig. 10. The XRD (a) and FT-IR (b) patterns for samples reclaimed from the buffer solution at different pH values (∗ indicates the $Al(OH)_3$ phase).

very well. This phenomenon can be explained by the possibility that the drug release is a co-effect behaviour, including dissolution of nanocomposites and ion-exchange between the intercalated anions in the lamella host and the phosphate anions in the buffer solution. In the case of the Bhaskar model linearity was obtained ($r = 0.9738$), compared with that of first-order model ($r = 0.9559$). We can suppose that the ion-exchange process is the main effect in the co-effect. The same kinetic models applied to release data at pH 7.45 were also considered. Fig. 9 shows the plots according to the first-order and Bhaskar equations with linear regression coefficients of 0.9891 and 0.9908, respectively. In this case, as in the previous one, the diffusion through the particle is the limiting step of the drug release. The fitting data primarily follow the experimental results.

In order to gain insight into the release mechanism of the present drug–LDH system, we subsequently reclaimed the resulting samples from the aqueous solutions after release test and submitted to XRD, FT-IR and ICP analysis. The XRD patterns for the reclaimed samples from pH 4.60 and 7.45 solutions are shown in Fig. 10a. Four sharp and symmetric lines in XRD patterns correspond to diffraction by planes (003), (006), (009) and (110), demonstrating the formation of a well-defined Mg–Al-LDH [6]. While comparing with Cpl-LDHs, the nanohybrid phase of Cpl-LDHs experienced a reduction in d_{003} value from 1.462 to 1.070 nm, which is quite similar to the d_{003} value of phosphate-containing LDHs [39], at both pH 4.60 and 7.45. This suggests that the ion-exchange between the intercalated anions and phosphate anions in the buffer may occur during the release process. The FT-IR analyses (Fig. 10b) show the broad band at ca. 1090 cm^{-1} due to the modes of δ(P–OH) and v_4(P–O), 847 cm^{-1} to v_1(P–O) and 780 cm^{-1} to v_4(P–O) [39,40], while the bands observed for Cpl-LDHs disappear. These findings are in good agreement with the XRD analyses. Furthermore, the ICP analysis of both reclaimed samples show that ~85% intercalated Cpl were released at the end of release test. While the content of Mg and Al decreases from 16.25% and 8.89% of initial Cpl-LDHs to 14.69% and 8.59% for pH 7.45 reclaimed sample, and to 12.74% and 8.59% for pH 4.60 one. Consequently, the Mg/Al ratio before and after release decreases from 2.06 to 1.93 (pH 7.45) and 1.52 (pH 4.60), indicating the occurrence of ion-exchange reaction and partial dissolution of LDH layer at weak acidic medium. Also, the partial dissolution of LDH layer at weak acidic medium, especially a little larger amount of Mg than Al dissolved during release process, probably result in the formation of $Al(OH)_3$ phase, consistent to the XRD analysis (∗ in Fig. 10a).

Based on above analyses, it is conceived that the sequence of events at pH 4.60 involves the rapid release of intercalated organic anions resulting from the dissolution of the LDH layer and the slow release step by ion exchange between the intercalated anions and phosphate anions in the buffer. However, the sequence of events at pH 7.45 involves only the ion-exchange process between the intercalated anions and phosphate anions in buffer.

4. Conclusions

Cpl-intercalated Mg–Al-LDHs with Mg/Al ratio of 2.06 as drug-inorganic composite has been successfully assembled by coprecipitation technique. The larger interlayer spacing of 0.982 nm for Cpl-LDHs determined by XRD analysis than the molecular size of Cpl (0.526 nm), together with FT-IR and Raman spectra analyses, suggest a vertical arrangement of Cpl disulphide-containing S–S bond between the layers with carboxylate anions to both hydroxide layers. The SEM analysis reveals the compact and non-porous structure of Cpl-LDHs composite with

approximately and linked elliptical particles of ca. 50 nm. The TG-DTA analysis demonstrates the obviously improved thermal stability of intercalated organic species after intercalating into LDH interlayer due to the host–guest interaction. The in vitro release studies of Cpl-LDHs show that both the release rate and release percentages are markedly decreased with increasing medium pH value. At pH 4.60, the release mechanisms involving dissolution at the beginning of release test followed by an ion-exchange mechanism result in a slower release rate of Cpl-LDHs after the first 1 min burst. At pH 7.45, the slower and persistent release process can be interpreted on the basis of the ion-exchange process between the intercalated organic anions and phosphate anions in buffer only. The present study may offer broad perspectives in utilizing Mg–Al-LDHs as an alternative biocompatible inorganic matrix for a feasible drug reservoir or a drug delivery carrier.

Acknowledgments

The authors thank financial support from the Ministry of Education Science and Technology Research Project of China (No. Key 104239), National Natural Science Foundation of China (No. 90306012) and National Basic Research Programme of China (973 Programme no. 2004CB720602).

References

[1] W.A. Lopes, H.M. Jaeger, Nature 414 (2001) 715.
[2] S.P. Newman, W. Jones, New J. Chem. (1998) 105.
[3] A.I. Khan, D. O'Hare, J. Mater. Chem. 12 (2002) 3191.
[4] V. Rives, M.A. Ulibarri, Coord. Chem. Rev. 181 (1999) 61.
[5] U. Costantino, M. Nocchetti, in: V. Rives (Ed.), Layered Double Hydroxides: Present and Future, Nova Science Publishers, New York, 2001, p. 383.
[6] F. Cavani, F. Trifiro, A. Vaccari, Catal. Today. 11 (1991) 173.
[7] J.H. Choy, S.Y. Kwak, J.S. Park, Y.J. Jeong, J. Mater. Chem. 11 (2001) 1671.
[8] J.H. Choy, S.Y. Kwak, Y.J. Jeong, J.S. Park, Angew. Chem. Int. Ed. 39 (22) (2000) 4041.
[9] S.Y. Kwak, Y.J. Jeong, J.S. Park, J.H. Choy, Solid State Ionics 151 (2002) 229.
[10] A. Burzlaff, S. Brethauer, C. Kasper, B.O. Jackisch, T. Scheper, Cytometry, Part A 62A (2004) 65.
[11] J.H. Choy, S.Y. Kwak, J.S. Park, Y.J. Jeong, J. Portier, J. Am. Chem. Soc. 121 (1999) 1399.
[12] S. Aisawa, S. Takahashi, W. Ogasawara, Y. Umetsu, E. Narita, J. Solid State Chem. 162 (2001) 52.
[13] Q. Yuan, M. Wei, D.G. Evans, X. Duan, J. Phys. Chem. B 108 (2004) 12381.
[14] T. Hibino, Chem. Mater. 16 (2004) 5482.
[15] N.T. Whilton, P.J. Vickers, S. Mann, J. Mater. Chem. 7 (8) (1997) 1623.
[16] H. Nakayama, N. Wada, M. Tsuhako, Int. J. Pharm. 269 (2004) 469.
[17] J.H. Meng, H. Zhang, D.G. Evans, X. Duan, Chem. J. Chin. Univ. 24 (2003) 1315 (in Chinese).
[18] J.H. Meng, H. Zhang, D.G. Evans, X. Duan, Chin. Sci. Bull. 50 (2005) 745.
[19] M.Z. bin Hussein, Z. Zainal, A.H. Yahaya, D.W.V. Foo, J. Control. Rel. 82 (2002) 417.
[20] V. Ambrogi, G. Fardella, G. Grandolini, L. Perioli, M.C. Tiralti, AAPS Pharm. Sci. Tech. 3 (2002) article 26.
[21] B.X. Li, J. He, D.G. Evans, X. Duan, Appl. Clay Sci. 27 (2004) 199.
[22] M.D. Arco, S. Gutierrez, C. Martin, V. Rives, J. Rocha, J. Solid State Chem. 177 (2004) 3954.
[23] M.D. Arco, E. Cebadera, S. Gutierrez, C. Martin, M.J. Montero, V. Rives, J. Rocha, M.A. Sevilla, J. Pharm. Sci. 93 (6) (2004) 1649.
[24] K.M. Tyner, S.R. Schiffman, E.P. Giannelis, J. Control. Rel. 95 (2004) 501.
[25] M. Wei, S.X. Shi, J. Wang, Y. Li, X. Duan, J. Solid State Chem. 177 (2004) 2534.
[26] H. Zhang, K. Zou, H. Sun, X. Duan, J. Solid State Chem. 178 (2005) 3485.
[27] J. Tronto, M.J.D. Reis, F. Silverio, V.R. Balbo, J.M. Marchetti, J.B. Valim, J. Phys. Chem. Solids 65 (2004) 475.
[28] A. Sintov, M. Simberg, A. Rubinstein, Int. J. Pharmacol. 143 (1996) 101.
[29] H.O. Ho, H.Y. Wang, M.T. Sheu, J. Control. Rel. 49 (1997) 243.
[30] A.O. Nur, J.S. Zhang, Int. J. Pharmacol. 194 (2000) 139.
[31] A. Torreggiani, P. Taddei, M.R. Tosi, V. Tugnoli, J. Mol. Struct. 565–566 (2001) 347.
[32] A. Tu, Proteins, Raman Spectroscopy in Biology, Wiley, Chichester, 1982 (p. 65).
[33] R.J. Kok, J. Visser, F. Moolenaar, D. de Zeeuw, D.K.F. Meijer, J. Chromatogr. B 693 (1997) 181.
[34] R.O. Macedo, T. Gomes do Nascimento, C.F. Soares Aragao, A.P. Barreto Gomes, J. Therm. Anal. Catal. 59 (2000) 657.
[35] F. Millange, R.I. Walton, D. O'Hare, J. Mater. Chem. 10 (2000) 1713.
[36] A.M. Fogg, J.S. Dunn, S.G. Shyu, D.R. Cary, D. O'Hare, Chem. Mater. 10 (1) (1998) 351.
[37] A.M. Fogg, J.S. Dunn, D. O'Hare, Chem. Mater. 10 (1) (1998) 356.
[38] R. Bhaskar, S.R.S. Murthy, B.D. Miglani, K. Viswanathan, Int. J. Pharmacol. 28 (1986) 59.
[39] U. Costantino, M. Casciola, L. Massinelli, M. Nocchetti, R. Vivani, Solid States Ionics 97 (1997) 203.
[40] M. Badreddine, M. Khaldi, A. Legrouri, A. Barroug, M. Chaouch, A. De Roy, J.P. Besse, Mater. Chem. Phys. 52 (1998) 235.